Effect of ciprofloxacin incorporation in PVA and PVA bioactive glass composite scaffolds

Mostafa Mabrouk, Amany Mostafa, Hassane Oudadesse, Azza A. Mahmoud, Mohamed I. El-Gohary

Effect of ciprofloxacin incorporation in PVA and PVA bioactive glass composite scaffolds

M. Mabrouk[a,b], A. A. Mostafa[a,b], H. Oudadesse[a], A.A. Mahmoud[c], and M. I. El-Gohary[d]

[a]Université de Rennes 1, UMR CNRS 6226, 263 av. du général leclerc, 35042 Rennes Cedex, France.
[b]Biomaterials Department ., National Research Centre NRC, Cairo, Egypt.
[c]Pharmaceutical Technology Department., National Research Centre NRC, Cairo, Egypt.
[d]Physics Department., Faculty of Science, Al -Azhar University, Cairo, Egypt.

Abstract

Scaffolds are implants used to deliver cells, drugs, and genes into the body in a local controlled release pattern which offers many advantages over systematic drug delivery. Composite scaffolds of polyvinyl alcohol (PVA) and quaternary bioactive glass (46S6 system) with different ratios of glass contents were prepared by lyophilisation technique. The broad spectrum antibiotic ciprofloxacin (Cip) was impregnated to the scaffold during the fabrication in a concentration of 5, 10 and 20%. Biodegradation rate and *in-vitro* mineralization of the prepared scaffolds were performed by soaking the scaffolds in simulated body fluid (SBF). Phase identification, microstructure, porosity, bioactivity, mechanical properties and drug release pattern in PBS were characterized by XRD, SEM coupled with EDS, Hg-porosimeter, inductively coupled plasma-optical emission spectroscopy (ICP-OES), universal testing machine, fourier transform infrared (FTIR) and UV-spectrophotometer, respectively. A porous scaffold has been obtained with porosity up to 85%. By increasing the glass contents in the prepared scaffold the porosity and the degradation rate decrease however, the compressive strength was enhanced. A sustained drug release pattern was observed with a quasi-Fickian diffusion mechanism. The formulated ciprofloxacin loaded porous polyvinyl alcohol scaffold gave an acceptable physicochemical properties and was able to deliver the drug in a prolonged release pattern which offers a distinguish treatment for osteomylitis as well as local antibacterial effect.

Keywords: Tissue engineering, scaffolds, ciprofloxacin, drug release, freeze drying, polyvinyl alcohol.

1. Introduction

Due to the increasing in population, there is a clinical demand for engineerined bone tissue. Tissue engineering is a promising field of bone repair and regenerative medicine in which cultured cells, scaffolds and osteogenic inductive signals are used to regenerate tissues. One of the present challenges in tissue engineering is the development of suitable scaffold materials that can be used as templates for cell adhesion, growth and proliferation [1]. Microorganisms that enter bone structures by spreading from the bloodstream or surrounding tissues or by direct contamination during trauma or surgery causes osteomyelitis [2]. A chronic osteomyelitis treatment protocol combines both surgical removing of dead bone tissue and prolonged parenteral or oral antimicrobial therapy [3–6]. The efficiency of systemic antimicrobial therapy is limited by poor drug accumulation in bone tissue, an impaired local immune response, and changes in bacterial growth rate, biofilm formation and intracellular location of the pathogens [4, 5]. Thus systemic treatment should be continued for at least six weeks, which causes important side effects and makes patient compliance difficult [6]. The production of implantable devices able to provide high levels of antimicrobial agents for a prolonged time at the infection site and with low level of side effects may improve the efficacy/safety ratio of the therapeutic strategies [7, 8].

Bioactive glass has many applications in bone tissue engineering, because of its known ability to bond strongly to bone and promote bone growth upon *in vivo* implantation [9]. When implanted in the body, bioactive glass induces an interfacial bioactive response. By contrast, *in-vitro*, it has been documented that the ionic products from the dissolution of the bioactive glass actually enhance osteoblast attachment, proliferation, differentiation and mineralization [10-12], as well as induce the differentiation of bone marrow stromal cells into mature extracellular producing osteoblasts [13]. Furthermore, the dissolution products of bioactive glass exert control over genetic factors of bone growth [14]. Nevertheless, bioactive glass, as compared to cortical and cancellous bone forms, tends to have weaker mechanical properties, especially in porous form. This fact restricts the use of these materials in a wide range of applications.

One approach to enhancing the mechanical properties of materials is the elaboration of inorganic–organic composites, as they often show an excellent combination between strength and toughness, as well as improved characteristics, when compared to their individual components.

Bioactive scaffolds were able to provide a three dimensional (3-D) architecture for enhancing osteogenesis and angiogenesis. Most of the scaffolds were built on complex constructs of several composition and additives. Natural polymer such as chitosan, alginate or gelatin [15-17] or synthetic polymer such as poly lactic acid (PLA), poly glycolic acid(PGA) an poly lactic –co-glycolic acid (PLGA) are widely used for polymer scaffold. However, some drawbacks still exist upon using polymers including: formation of acidic species, this leads to a decrease in pH and tissue inflammation [18, 19]. Among several choices of polymers, poly (vinyl alcohol) (PVA), a hydrophilic semicrystalline polymer, has been frequently explored as an implant material in wide array of biomedical applications such as drug delivery systems, wound dressings, membranes, surgical repairs and artificial skin, mainly due to its excellent mechanical strength, biocompatibility, and nontoxicity [15, 16].

Direct application of antibiotics or growth factors to the defect site and the control release of the drug delivery systems have been developed [20, 21]. Antibiotics can be incorporated into bone substitutes [22]. The sustained release of antibiotics from scaffold structures has been widely demonstrated to control the kinetic of the release [23]. Drug releasing polymer scaffolds should have certain criteria such as a homogeneity of the drug distribution, good binding affinity of the drug to the scaffold, define amount of the drug loading as well as release kinetic and stability [23-25]. The most widely acceptable agents in local delivery system for chronic osteomylitis are amino glycosis and quinolones. Ciprofloxacin (1-cyclopropyl-6-fluro-1, 4-dihydro-4-oxo-7- (1-pipera Zinyl)-3- quinoline carboxylic acid) is a fluroquinolone derivative, widely used in osteomyelitis because of its favorable penetration and bactericidal effect on all the probable osteomyelitis pathogens [29]. The main purpose of the current study was to develop and fabricate a construct of bioactive scaffold combining an antibiotic (ciprofloxacin). Bioactive glass powders were used as powder fillers to reinforce poly

vinyl alcohol scaffold. Characterization of these scaffolds before and after addition of the drug has been investigated by TEM, XRD, FTIR, mercury prosimeter, SEM coupled with EDS, ICP-OES, universal testing machine and UV-spectrophotometer. Bioactivity of the composite scaffolds and their use as drug carriers to effectively deliver therapeutic agent in a sustained and controlled manner has been studied.

2. Materials and methods

2.1. Fabrication of PVA/SG-B –Cip scaffolds

46S6 bioactive glass powder was synthesized by sol-gel method SG-B as following.
A colloidal solution of 46S6 was prepared by sol-gel. Initially, 56 ml of tetraethoxysilane (TEOS:Fluka, Mwt=208.33) was added to 350 ml of distilled water and 350 ml of ethanol at room temperature . pH was adjusted at 2 by nitric acid with continuous stirring for 1hr, addition of 24.5 g of calcium nitrate hydrate (Fluka, Mwt=236) to the above solution continue stirring till dissolving, addition of 21.07 g of sodium hydroxide (Prolab, Mwt= 40) to the above mixture (the previous mixture was named solution A), 10 g of polyethylene glycol (PEG-Fluka Mwt=600) was dissolved in 400 ml of distillate water at room temperature. 3.43 g of ammonium dihydrogen phosphate (MERK, Mwt=115.03) was added to the PEG solution, this mixture was named solution B. Furthermore, solution (B) was gradually added on solution (A) with continuous stirring over night. The resulted solution was filtrated and washed with distillate water for 3 times and with ethanol for 1 time using centrifuge with 1650 rpm for 10 min drying of the washed gel at 70°C for overnight. The dried powder was calcinied at 600^{o}C for 2hr.

2.1.1. Composite preparation

PVA/SG-B-Cip composite scaffolds were prepared by employing freeze drying technique as demonstrated in figure (1.1). Firstly, PVA (ALDRICH, Mwt= 67.000) was dissolved in distilled water at 80^{o}C for 2hr using a polymer concentration of 15 wt%. Three different concentrations of SG-B (nano particles see TEM image figure (1.2)) 33.5,50 and

66.5 wt%, were added to the PVA solution and continue stirred for overnight using a magnetic stirrer in order to break the SG-B agglomerates and ensure a better (homogenous) distribution of SG-B particles in the composite scaffolds. Three different concentrations of ciprofloxacin 5, 10 and 20 wt% were added to the above mixture continue stirred for 1hr (scaffolds with the same composition was prepared without drug loading as a control). Scaffolds were casted in Teflon molds and kept at -18^{o}C for overnight, and freeze dried for 24 hr then the scaffolds were removed from the molds and kept in the desecrator for further analysis as mentioned below.

2.2. Morphological and microstructural properties

The microarchitecture of these scaffolds was assessed qualitatively using scanning electron microscopy (SEM) and quantitatively using mercury intrusion porosimetry (MIP) and liquid displacement method.

2.2.1. SEM

SEM analyses were performed on a thin piece of scaffold sheared from the center using a sharp razor blade after soaking in liquid nitrogen for 2 minutes. Scaffolds were observed using (max. of 20 kV) SEM with gold palladium coating to avoid beam damage of the polymer, which can be prominent on these scaffolds that have very fine microstructure.

2.2.2. MIP

MIP was performed using (PORESIZER 9320 V2.08) to determine median pore diameter, and percent porosity.

2.2.3. Liquid displacement method

Scaffold samples were submersed in cyclohexan for 1 hr. The volume of a scaffold immersed in the fluid is equal to the volume of the displaced fluid, and we can calculate the porosity from the following equation:

$$P\ \% = [(W_1-W_3)/ (W_2-W_3)] \times 100 \qquad (1)$$

Where W_1: weight of the scaffold before immersion, W_2: weight of the scaffold after immersion and W_3: weight after drying by this method we can just get the porosity percentage (P %).

2.3. Mechanical properties of the prepared scaffolds

Bones are often submitted to compression stress in the body. It has been broadly accepted by the research community to perform compression assays for evaluating biomaterials for potential use as bone repair. For that reason, the mechanical behavior of the composites was evaluated by compression tests. Specimens were evenly cut from the most homogeneous region of the foam to form blocks measuring 10 × 10 × 10mm^3. These samples were positioned between parallel plates using equipment EMIC DL 3000 and compressed with a crosshead speed of 0.5$mm \cdot min^{-1}$ and a 1.0 kN load cell. At least three samples (n = 3) of each hybrid system were measured and the results averaged. Compressive strength tests were carried out to determine the effect of bioactive glass and the drug concentrations on the mechanical strength of scaffolds.

2.4. Bioactivity

2.4.1. Phase analysis by X-ray diffraction (XRD).

X-ray diffraction (XRD) technique (PhilipsX'Pert-MPD system with a CuKa wavelength of 1.5418A°) was used to analyze the structure of the prepared SG-B and PVA/ SG-B composite scaffolds. The diffract meter was operated at 40kV and 30mA at a 2ɵ range of 10–70°employing a step size of 0.058/s.

2.4.2. Infrared studies

Fourier transformed infrared analysis (FTIR; Nicolet Magna-IR 550 spectrometer, Madison, Wisconsin) was performed to identify the nature of the chemical bonds between atoms. The samples were small pellets, of 0.5 cm diameter, obtained by pressing the scaffolds powder with KBr.

2.4.3. SEM coupled with EDS

The morphology of surfaces of scaffolds was studied by using scanning electron microscopy (SEM) (Jeol JSM 6301). It is a technique of morphological analysis based on the principle of electron-matter interactions. To allow surface conduction, the scaffolds were metalized by gold-palladium layer (a few μm of thickness) before being introduced into the analysis room. Semi quantitative chemical analysis on scaffolds surfaces after immersion in SBF, covered by gold-palladium layer to allow surface conduction, was performed by energy dispersive spectroscopy (EDS) in Jeol JSM 6400.

2.4.4. ICP-OES

The concentrations of (Ca, p and Si) elements after each soaking time in SBF were measured by using Inductively Coupled Plasma-Optical - Emission Spectrometry (ICP-OES). This method offers a high sensitivity, less than 1μg/g depending on the analyzed matrix and offers a high accuracy. The principle is based on the determination of the amount of each element present in solution by analyzing the intensity of the radiation emitted at the specific elemental frequency after the nebulisation of atoms.

2.5. In vitro degradation studies

The degradation pattern of the composite scaffold was studied in PBS medium at 37 ◦C. groups of scaffolds (3 scaffolds in each) were immersed in PBS and incubated for up to 30 days. After each period time one of the scaffolds was washed two times by distilled water to remove ions adsorbed on the surface and was dried. Initial weight of the scaffold was noted as Wo and dry weight as Wt. The degradation of scaffolds was calculated using the following formula:

$$\text{Degradation } \% = (Wo - Wt)/Wo \times 100 \qquad (2)$$

2.6. Ciprofloxacin release behavior

Drug incorporation into the scaffolds was investigated by means of XRD, FTIR and SEM coupled with EDS.

Phosphate buffer solution (PBS), pH 7.4 (10 ml), previously heated at 37°C, was added to test tubes containing freshly prepared scaffolds. The tubes were kept at 37°C with shaking (50 oscillations min^{-1}) and, at pre-established times, 1 ml samples of the release medium were taken and the drug concentration was determined spectrophotometrically at 277 nm (Jenway 6705 UV/Vis, UK). The samples were replaced with fresh buffer in order to keep constant volume of medium. All experiments were carried out in triplicate. Ciprofloxacin release was monitored for 360 hr.

2.7. Mechanism of ciprofloxacin release

Korsmeyer–Peppas model [31] was used to find out the mechanism of drug release from the investigated scaffolds:

$$M_t / M_\infty = Kt^n \quad (3)$$

Where, M_t / M_∞ is fraction of drug released at time t, k is the rate constant and n is the release exponent. In case of quasi-Fickian diffusion the value of $n < 0.5$, Fickian diffusion $n = 0.5$, non-Fickain or anomalus transport $n = 0.5\text{-}1.0$ and Case II transport $n = 1.0$.

3. Results and discussion

3.1. Morphological and microstructural properties

The effect of the particle size of SG-B particles on the properties of PVA/SG-B scaffolds, which are being developed for tissue engineering applications [32]. The morphology of the prepared scaffolds is presented in (figure 2); in which we can observe that all the prepared scaffolds have wide range of interconnected pores including macro, micro and nanopores as it also confirmed by mercury porosimeter. PVA scaffold shows highly interconnected pores with smooth pore walls. Incorporation of ciprofloxacin into the PVA scaffold changes the arraying and shapes of pores and its thickness due to the interaction between ciprofloxacin and PVA. As the glass content increases the porosity decreases and the pore walls becomes thicker. Among several processing techniques, the freeze drying method was chosen since it could provide easy control of the pore structure [33]. The co-existence of macropores and micropores is not only favorable for the ingrowth of cells and new tissue but also beneficial to the exchange of nutrients and metabolic waste [34]. The porosity percentage for the prepared scaffolds was determined by MIP and liquid displacement methods and there was no significant difference between the two methods as it is demonstrated in table (1) [32].

3.2. Mechanical properties

The mechanical behavior of the prepared scaffolds was characterized by determining the compressive strength. The PVA alone exhibit low compressive strength as shown in figure (3). In the produced scaffolds, a marked change could be observed, as the amount of glass and drug increased the compressive strength increase. The incorporation of SG-B into PVA polymer enhances the compressive strength, due to their small particle size and large surface area which results in great attachment of SG-B particles to the polymer matrix as reported before [33-38].

3.3. Bioactivity

Figures (4) and figure (5) represent XRD and FTIR respectably of the prepared PVA/SG-B composite scaffolds with SG-B and PVA as references before immersion in SBF.

3.3.1.1. X-ray diffraction analysis and FTIR before immersion in SBF

The X-ray diffraction analysis result from the pure bioactive glass is as expected it did not show the presence of any crystalline phase, being totally amorphous. On the other hand, the XRD patterns from both samples of pure PVA and composite scaffolds have shown some diffraction bands. Hence, it has being identified as a semi-crystalline structure due to the superior concentration of hydroxyls groups. The XRD curve for PVA/SG-B can be directly verified the sum up of both contributions from PVA with semi-crystalline structure and amorphous phase of SG-B [39]. It can be noted for two peaks for PVA/SG-B at 2θ of 26.6° (113) and 33.64° (131), which indicated some degree of crystallinity on the biopolymer network which diminish with increase of the glass content. That would be a typical XRD pattern for the scaffold showing contribution from all components in the system [40, 41].

The contribution of each and every component on the final produced scaffold network was confirmed by FTIR. Hence, the broad band observed from 3200 to 3550 cm^{-1} in the PVA spectra assigned to hydroxyls (νOH) stretching due to the strong hydrogen bond of intramolecular and intermolecular type [42-43]. Also, the strong band at 2870–2950 cm^{-1} was attributed to alkyl stretching mode (νCH). The bands ranging from 1710 to 1750 cm^{-1} and 1200 to 1275 cm^{-1} arise due to the stretching vibration of carbonyl (νC=O) and ester, respectively, from the vinyl acetate group found in partially hydrolyzed PVA polymer . Some other bands which can be found related to PVA are located at 1410–1460 cm−1 assigned to δ(CH)CH2; 1200–1270 cm^{-1} of group ν(C–O)–C–OH; 820–850 cm^{-1} from alkyl chain backbone [42-45]. In an analogous analysis, the FTIR spectrum of the SG-B presented the bands related to Si–O–Si asymmetric and symmetric stretching modes at approximately 1100 cm^{-1} and 800 cm^{-1}, respectively [35–36]. There is an overlapping of the bands in the range from 900 to 1500 cm^{-1} derived from the bioactive glass and the PVA components [42-45]. It is worth noting that the composite formation leads to the broadening of the bands related to vinyl acetate copolymer, that almost disappear as a consequence of the hydrogen bonds involving C=O groups and silanol groups in silicate networks [48].

3.3.1.2. X-ray diffraction analysis and FTIR after immersion in SBF

The XRD of the prepared scaffolds after soaking in SBF for different time intervals demonstrated in figure (6). The calcium phosphate layer formed on the surface of PVA/SG-B is crystallized after three weeks of immersion in the SBF as documented before [49]. Indeed after 2 days of immersion, the peaks of crystallization related to the layer of HA formed on the surface of PVA/SG-B starts to appear and intensity increase progressively versus the time of immersion and SG-B content. After 21 days of soaking in SBF, the XRD pattern show rays with maximum at about 32°. These peaks corresponding respectively to (211), (310) and (203) reticular plan and highlight the apatite like layer [49-51].

Figure (7) The IR spectrum of synthetic hydroxyapatite is used as references to evaluate the structural evolution and the bioactivities of the prepared scaffolds. After soaking in SBF solution, the initial characteristic bands of PVA/SG-B biocomposite are modified strongly because of the interfacial reactions scaffolds and the SBF. Consequently, the spectra of these biomaterials reveal new bands [51].

In detail, the spectrum of PVA/SG-B scaffold after 2 days of soaking in SBF shows three new well-defined phosphate bands at 565, 603 and 1039 cm^{-1}. They are assigned to stretching vibrations of PO_4^{3-} group in phosphate crystalline phases with low intensity due to great bounding affinity between SG-B and PVA due to this fact a relative slow reaction between PVA/SG-B scaffolds and SBF tacking place. This result confirms the formation of a calcium phosphate layer; this spectrum is quite similar to that of hydroxyl apatite except two bands located at 1620 and 3423 cm^{-1}. These bands are characteristic of the presence of water related to the hygroscopic feature of the formed apatite. In addition, the carbonate band at 1420 cm^{-1} is also observed. This band attributes to a stretching vibration of the C-O liaisons in carbonate groups. The presence of carbonate bands indicates the formation of a layer of carbonated hydroxyapatite on the surface of PVA/SG-B biocomposite. The obtained results highlight the rapid formation of apatite layer on the surface of PVA/SG-B biocomposite. In addition, PVA/SG-B scaffolds reveal three Si-O-Si bands at 470 cm^{-1} (bending vibration), 799 cm^{-1} (bending vibration) and 1075 cm^{-1} (stretch vibration). These confirm the presence of a silica gel [30]. The

appearance of apatite mineral and a silica gel indicate the interactions between the scaffolds and SBF as described by Hench et al. This mechanism could be explained through the following steps:

(a) rapid exchange of protons H_3O^+ from the SBF with Ca^{2+} , Na^+ ions in bioglass to form the Si-OH groups, (b) loss of soluble silica as $Si(OH)^4$ by breaking of Si-O-Si bridging links and subsequent formation of surface silanol groups in the process, (c) condensation and repolymerization of surface silanols to form SiO_2-rich surface layer, (d) migration of Ca^{2+} and PO_4^{3-} through the surface silica-rich layer and formation of a Ca-P rich layer on the surface of biocomposite, (e) incorporation of OH^-, CO_3^{2-} from the solution and subsequent crystallization of the Ca-P layer to form HCA [53-56]. The obtained results confirm the bioactivity of PVA/BG biocomposite. Especially, they highlight the positive effect of SG-B particle size and SG-B bounding strength with PVA controls the formation rate of well crystallized apatite layer on its surface.

3.2.2. SEM with EDS after immersion in SBF

Two compositions of the prepared scaffolds have been under investigated by SEM coupled with EDS , figure (8), to evaluate their surface changes after soaking in SBF for 21 days (PV and 1PVA:2SG-B). This scaffolds had exhibit excellent bioactivity and high fracture toughness. The hydroxy apatite crystals formed with condensed manure on the surface of the biocomposite scaffolds but the surface of PVA scaffold is not changed yet. Incorporation of PVA with SG-B induces a great modification to PVA bioactivity. SEM analysis suggested the excitants of strong molecular interaction between SG-B particles and PVA network, causing SG-B to be dispersed uniformly in the composite scaffolds. The presence of Ca, P, Na and Cl elements on the surface of the prepared composite scaffolds were determined by EDS. The phosphocalcic ratio Ca/P after 21 days of immersion in SBF is nearly equal to the stoichiometric apatite [33, 49 and 57-60].

3.3.3. Evaluation of elemental concentrations in SBF

The change of ions concentrations in SBF was demonstrated in figure (9). For P and Si ions they take the same behavior for all the prepared scaffolds with little difference in

their amount in the SBF. Which is due to the limit of the integrate combination between SG-B and PVA. This little difference is according to bounding and incorporation of SG-B into PVA. The SG-B particle size is affecting on the amount of P and Si in the SBF as its confirmed by XRD, FTIR and SEM with EDS. The ions concentration of Ca was found to be completely different for each composition of scaffolds. This is much believed to be according to the glass content in the scaffolds and the small particle size of SG-B as they in turn changes the porosity and the degradation rate in the SBF [35, 49, 50, 54, 57, 58, and 59].

3.4. Degradation

Biodegradation rate of the prepared scaffolds was investigated in SBF at different time intervals with PVA alone as control as shown in figure (10). PVA scaffold exhibit higher degradation rate (100% after 2 days) than those of PVA/SG-B scaffolds. Ideally, in tissue engineering, a scaffold is usually intended to temporary fill a defect, while gradually degrading as neo-tissue is formed. In due course, the scaffold is replaced by new bone tissue [61]. After implantation, the scaffold interacts with the tissue fluids, uptaking them at some extent, starting the degradation process [62]. A relative low degradation rate is much favorable for cell attachment and differentiation. Furthermore, increases of the glass amount in the scaffold decreases the degradation rate due to the fact that incorporation of inorganic filler into polymer matrix decreases the porosity as confirmed by MIP and liquid displacement methods and as documented before [63 and 64]. Porosity decrease lead to decreases of the exposed surface area from the scaffold to the SBF. This decreasing prolong the consumed time for biodegradation, giving more time for cells attachment and proliferation [65].

3.5. Ciprofloxacin incorporation

The success of incorporation of ciprofloxacin into PVA and PVA/SG-B scaffolds was confirmed by XRD, FTIR and SEM coupled with EDS.

3.5.1. XRD

Figures (11.1) represent the XRD for PVA and PVA/SG-B scaffolds with and without the drug. Ciprofloxacin has specific sharp crystal peaks while PVA, SG-B and PVA/SG-B have broad peaks. When ciprofloxacin was entrapped into the scaffold matrix, its sharp crystal peaks were overlapped with the noise of the surrounded polymer and disappeared indicating that ciprofloxacin was successfully entrapped into the scaffold matrix system and formation of a new solid phase for ciprofloxacin with low crystallinity[66-70].

3.5.2. FTIR

The FTIR for ciprofloxacin loaded scaffolds are demonstrated in figures (11.2). The FTIR spectrum of ciprofloxacin shows one prominent characteristic band between 3500 and 3450 cm^{-1}, which was assigned to stretching vibration of OH groups Another band at 3000- 2950 cm^{-1} represent alkene and aromatic C-H stretching, mainly υ=C-H was demonstrated. The 1950 to 1450 cm^{-1} region exhibited FTIR absorption from a wide variety of double-bonded functional groups. The band at 1750 to 1700 cm^{-1} represented the carbonyl C=O stretching i.e., υ**C=O**. The peak between 1650 and 1600 cm^{-1} was assigned to quinolones. The band from 1450 to 1400 cm^{-1} represented υ**C-O** and at 1300 to 1250 cm^{-1} suggested bending vibration of O-H group which proved the presence of carboxylic acid. A strong absorption band between 1050 and 1000cm^{-1} was assigned to C-F group. The FTIR for the PVA scaffolds loaded with ciprofloxacin indicate the presence of new bands at 3522, 1744, and 1473.52 cm^{-1} when compared with those of non-medicated scaffold due to the presence of ciprofloxacin. These bands were indicated also for PVA/SG-B scaffolds loaded with ciprofloxacin beside another band at 1088 cm^{-1} with high intensity due to combination of drug with glass particles into the polymer matrix. A shorter band appeared in the region of 1500–1200 cm^{-1} that could be ascribed to the hydrated bonds with ciprofloxacin molecules [66-73].

The FTIR spectra indicate that, although a physical interaction between the drug and the scaffold components occurs with both PVA/SG-B scaffolds. This is probably because PVA/SG-B has a greater content of pendant hydroxyl groups that are more accessible for establishing hydrogen bonds with the drug [69].

3.5.3. SEM coupled with EDS

The SEM image of the drug shows rod shape crystals and its EDS indicate the presence of F and Cl elements which are the main components of the drug as demonstrated in figure (11.3). SEM images for the cross-section of scaffold loaded with the ciprofloxacin reveal the rod shape of ciprofloxacin crystal in the scaffold matrix system [70, 75]Also the EDS confirm the presence of F and Cl elements in the scaffolds loaded with ciprofloxacin . Therefore, XRD, FTIR and SEM coupled with EDS indicate and confirm the success incorporation of ciprofloxacin into PVA and PVA/SG-B scaffolds.

3.6 Release behavior of ciprofloxacin

The release behavior of ciprofloxacin from the prepared scaffolds is presented in figure (12). Considering the hydrophilic molecule, ciprofloxacin is expected to exhibit burst release from the investigated system. Moreover, a sustained drug release profile was observed form the investigated figures with quasi-Fickian diffusion mechanism (n-values less than 0.5). This mechanism indicates that the polymer is hydrated, swell and then the drug diffuses through the swollen matrix system, which ultimately slows down the kinetic release.

The release profile for ciprofloxacin from scaffold prepared from PVA/SG-B loaded with 5, 10 and 20% ciprofloxacin was higher than that for scaffold loaded with PVA scaffolds loaded with 5, 10 and 20% of ciprofloxacin. This could be due to the interaction between PVA alone with ciprofloxacin resulting in great bounding affinity between the drug and PVA polymer. On the other hand presence of SG-B particles in the polymer matrix leaves no free space for the ciprofloxacin causing fast release for the drug in the PBS. [67, 71 and 75].

Conclusions

In this study, the PVA/SG-B biocomposite scaffolds loaded with ciprofloxacin with well interconnected pore structure were fabricated via freeze drying technique. The degradation rate and physicochemical properties of the prepared scaffold by freeze drying for tissue engineering could be controlled by controlling glass content and drug concentrations. The pore size achieved is suitable for cell activation and tissue regeneration. Drug loaded scaffolds with ciprofloxacin exhibit a good drug delivery system with sustained drug release. The biodegradation rate and structural morphology of the prepared scaffolds could be controlled by adjusting ciprofloxacin percentage.

References

[1]. Kretlow, J. D. and Mikos, A. G.: from material to tissue biomaterial development, scaffold fabrication, and tissue engineering. J AIChE 2008; 54**:** 3048–67.

[2]. Brook, I.: Microbiology and management of joint and bone infections due to anaerobic bacteria. J Orthop Sci 2008; 13:160–9.

[3]. Makinen, TJ., Veiranto, M. and Lankinen, P.: In vitro and in vivo release of ciprofloxacin from osteoconductive bone defect filler. J Antimicrob Chemother 2005; 56:1063–8.

[4]. Brady, RA., Leid, JG. and Calhoun, JH.: Osteomyelitis and the role of biofilms in chronic infection. FEMS Immunol Med Microbiol 2008; 52:13–22.

[5]. Garcia-Lechuz, J. and Bouza, E.: Treatment recommendations and strategies for the management of bone and joint infections. Expert Opin Pharmacol 2009; 10:35–55.

[6]. Lazzarini, L., Lipsky, BA. and Mader, JT.: Antibiotic treatment of osteomyelitis: what have we learned from 30 years of clinical trials. Int J Infect Dis 2005; 9:127–38.

[7]. Kanellakopoulou, K.: Local treatment of experimental seudomonas aeruginosa osteomyelitis with a biodegradable dilactide polymer releasing ciprofloxacin. Antimicrob Agents Chemother 2008; 52:2335–9.

[8]. Lepretre, S.: Prolonged local antibiotics delivery from hydroxyapatite functionalised with cyclodextrin polymers. Biomate 2009; 30:6086–93.

[9]. Hench, L. L.: Genetic design of bioactive glass. J Eur Ceram Soc 2009**; 7:** 1257–65.

[10]. Kaufmann, E. E., Ducheyne, P. and Shapiro I.: Effect of varying physical properties of porous, surface modified bioactive glass 45S5 on osteoblast proliferation and maturation. J Biomed Mater Res 2000; 52: 783–96.

[11]. Jones, J. R., Tsigkou, O. and Coates, E. E. : Extracellular matrix formation and mineralization on a phosphate-free porous bioactive glass scaffold using primary human osteoblast (HOB) cells. Biomate 2007; 28: 1653–63.

[12]. Valerio, P., Pereira, M. M. and Goes, A. M.: The effect of ionic products from bioactive glass dissolution on osteoblast proliferation and collagen production. Biomate 2004; 25: 2941–8.

[13]. Radin, S., Reilly, G. and Bhargave, G.: Osteogenic effects of bioactive glass on bone marrow stromal cells. J Biomed Mater Res A 2005; 73: 21–9.

[14]. Xynos, I. D., Buttery, L. D. and Hench L. L.: Ionic products of bioactive glass dissolution increase proliferation of human osteoblasts and induce IGF II m RNA expression and protein synthesis. Biochem Biophys Res Commun. 2000; 276: 461–5.

[15]. Yilgor, P., Tuzlakoglu, K., Reis, R.L., Hasirci, N. and Hasirci, V.: Incorporation of a sequential BMP-2/BMP-7 delivery system into chitosan-based scaffolds for bone tissue engineering, Biomate 2009;30: 3551–9.

[16]. Xu, J., Li J.B, Lian, X., Ayers, D.C. and Song, J.: Sustained and localized in vitro release of -2/7, RANKL, and tetracycline from FlexBone, an elastomeric osteoconductive bone substitute, J Orthop Res. 2009; 27:1306– 11.

[17]. Choi, D.H., Park, C.H., Kim, I.H., Chun, H.J., Park, K. and Han, D.K., Fabrication of core-shell microcapsules using PLGA and alginate for dual growth factor delivery system, J. Control. Release 2010; 147:193–201.

[18]. Mikos AG, McIntire LV, Anderson JM and Babensee JE.: Host response to tissue engineered devices. Adv Drug Deliv Rev 1998; 33:111–39.

[19]. Böstman O, Hirvensalo E, Vainionpää S, Mäkelä A, Vihtonen K and Törmälä P, Ankle fractures treated using biodegradable internal fixation. Clin Orthop Relat Res 1989; 238:195–203.

[20]. Chen, R.R. and Mooney, D.J.: Polymeric growth factor delivery strategies for tissue engineering, Pharm. Res. 2003; 20: 1103–12.

[21]. Han, D., Liu, W., Ao, Q., Wang, and G.: Optimal delivery systems for bone morphogenetic proteins in orthopedic applications should model initial tissue repair structures by using a heparin-incorporated fibrin-fibronectin matrix, Med. Hypotheses 2008;71: 374–8.

[22]. Silverman, L.D., Lukashova, L., Herman, O.T., Lane, J.M. and Boskey, A.L., Release of gentamicin from a tricalcium phosphate bone implant, J. Orthop. Res. 2007; 25: 23–29.

[23]. Sokolsky-Papkov, M, Agashi, K, Olaye, A, Shakesheff, K and Domb, AJ. Polymer carriers for drug delivery in tissue engineering. Adv Drug Deliv Rev 2007; 59:187–206.

[24]. Griffith, LG and Naughton, G. Tissue engineering-current challenges and expanding opportunities. Sci 2002; 295:1009–14.

[25]. Nair, LS and Laurencin, CT. Polymers as biomaterials for tissue engineering and controlled drug delivery. Adv Biochem Eng Biotechnol 2006; 102:47–90.

[26]. Yamaoka, T., Tabata, Y. and Ikada, Y.: Comparison of body distribution of poly (vinyl alcohol) with other water-soluble polymers after travenous administration. J Pharma and Pharmaco 1995; 47 no. 6:479–86.

[27]. Chiellini, E., Corti, A., D'Antone, S. and Solaro, R.: Biodegradation of poly (vinyl alcohol) based materials. Progr in Polym Sci, 2003; 28, no. 6: 963–1014.

[28]. Alta, V., Bitschnaua, A. and Osterlinga, J.: The effects of combined gentamicin–hydroxyapatite coating for cementless joint prostheses on the reduction of infection rates in a rabbit infection prophylaxis model. Biomate. 2006; 27: 4627-34.

[29]. Nayak, A. K. and Sen, K. K.: Hydroxyapatite-ciprofloxacin minipellets for bone-implant delivery: Preparation, characterization, in-vitro drug adsorption and dissolution studies. Int J Drug Dev Res 2009; 1: 47–59.

[30]. Dietrich, E., Oudadesse, H., Lucas-Girot, A. and Mami, M.: In vitro bioactivity of melt-derived glass 46S6 doped with magnesium. J of Biomed Mater Res. 2009; 88: 1087-96.

[31]. Korsmeyer, R. W., R. Gurny, et al. (1983). "Mechanisms of solute release from porous hydrophilic polymers." Int J Pharm15: 25-35.

[32]. Misra, SK., Nazhat, SN. and Valappil, SP.: Fabrication and characterization of biodegradable Poly (3-hydroxybutyrate) composite containing bioglass. Biomacromolecules 2007; 8:2112-9.

[33]. Yazdanpanah, A., Reza, K. and Moztarzadeh, F.: Enhancement of the fracture toughness in bioactive glass-based nanocomposites with nanocrystalline forsterite as advanced biomaterials for bone tissue engineering applications. Ceram Inter 2012; 38:5007-14.

[34]. Wong Sh., Baji, A. and Alan, N.: Effect of specimen thickness on fracture

toughness and adhesive properties of hydroxyapatite-filled polycaprolactone. Compos : Part A, 2008; 39: 579–87.

[35]. Julian, R. J.: New trends in bioactive scaffolds: The importance of nanostructure. J Eur Cer Soci. 2009; 29: 1275–81.

[36]. Nallaa, R.K., Kinneyb, J.H., and Ritchie R.O.: Effect of orientation on the in vitro fracture toughness of dentin: the role of toughening mechanisms. Biomate 2003; 24:3955–68.

[37]. Mahinda, D. K. and Ken, P. Ch.: Fracture toughness testing of brittle materials using semi-circular bend (SCB) specimen. Engi Fract Mech , 2012; 91: 133–50.

[38]. Cook, R.B., Curwen, C., Tasker, T. and Zioupos, P.: Fracture toughness and compressive properties of cancellous bone at the head of the femur and relationships to non-invasive skeletal assessment measurements. Med Engi & Phy , 2010; 32: 991–7.

[39]. María, C., Gutiérrez, Zaira Y., Carvajal, G. and Jobbágy M.: Poly (vinyl alcohol) Scaffolds with Tailored Morphologies for Drug Delivery and Controlled Release. Adv Funct Mater. 2007; 17: 3505–13.

[40]. Hutmacher, DW.: Scaffolds in tissue engineering bone and cartilage. Biomate 2000; 21:2529–43.

[41]. Tao, W., Mahir, T. and Gunasekaran, S.: Selected properties of pH-sensitive, biodegradable chitosan–poly (vinyl alcohol) hydrogel, Polym. Int. 2004; 53: 911–8.

[42]. Andrade, G., Barbosa-Stancioli, E. F., Mansur, A. A. Piscitelli, W Vasconcelos, L. and Mansur H. S.: Design of novel hybrid organic-inorganic nanostructured biomaterials for immunoassay applications,". Biomed Mate , 2006; 1, no. 4: 221–34.

[43]. Mansur, H.S. and Costa, H. S.: Nanostructured poly(vinyl alcohol)/bioactive glass and poly(vinyl alcohol)/chitosan/ bioactive glass hybrid scaffolds for biomedical applications,". Chem Engi J . 2008; 137, no. 1: 72–83.

[44]. Mansur, H. S., Or´efice, R. L. and Mansur, A. A.: Characterization of poly (vinyl alcohol)/poly (ethylene glycol) hydrogels and PVA-derived hybrids by small-angle X-ray scattering and FTIR spectroscopy,". Poly, 2004; 45, no. 21: 7193–02.

[45]. Coates, J.: Encyclopedia of analytical chemistry: interpretation of infrared spectra, a practical approach," in *Encyclopedia of Analytical Chemistry*, R. A. Meyers, Ed., 2000; JohnWiley & Sons, Chichester, UK, 10815–37.

[46]. Almeida, R. M. and Pantano, C. G.: Structural investigation of silica gel films by infrared spectroscopy. J App Phy, 1990; 68, no. 8: article 4225, 8 pages.

[47]. Wang, T., Turhan, M. and Gunasekaran, S.: "Selected properties of pH-sensitive, biodegradable chitosan-poly(vinyl alcohol) hydrogel," Poly Int. , 2004; 53, no. 7: 911–8.

[48]. Shin, S.-H. and Kim, H.-I.: Contribution of hydrogen bond and coupling reaction improvement in compatibility of organic polymer/silica nanocomposites,". Ind. & Engi Chem Res., 2001; 7: 147–52.

[49]. Mami, M., Oudadesse, H. and Doebez-Sridi, R.: Synthesis and in-vitro characterization of melt derived 47S $CaO–P_2O_5–SiO_2–Na_2O$ bioactive glass. Ceram − Silik .2008; 52 (3):121-9.

[50]. Oudadesse, H., Mami, M. and Doebez-Sridi, R.: Study of the Bioactivity of Various Mineral Compositions of Bioactive Glasses. Bioceram Develop and App. 2011; 1: Article ID D110151, 3 pages.

[51]. Superb, K. M., Dirk, M. and Brunner Tobias, J.: Comparison of nanoscale and microscale bioactive glass on the properties of P(3HB)/Bioglass composites. Biomat. 2008; 29: 1750-61.

[52]. Luo, P.: Methods of synthesizing hydroxyapatite powders and bulk materials. United States Patent 1999.

[53]. Hench, L.L., Splinter, R.J., Allen, W.C. and Greenlee, T.K.: Bonding mechanisms at the interface of ceramic prosthetic materials. J Biomed Mater Res 1971, 5(6), pp. 117-41.

[54]. Oudadesse, H., Mami, M., Doebez-Sridi, R., Pellen, P., Perez, F., Jeanne S., Chauvel-Lebret D., Mostafa A. and Cathelineau G., Study of various mineral compositions and their bioactivity of bioactive glasses. Biocera 2009;22 : 379-82.

[55]. Hench, L. L., The story of bioglass. J Mater Sci: Mater Med 2006; 17: 967-78.

[56]. Hench, L.L. and West, J.K.: Biological applications of bioactive glasses, Life Chem Rep 1996, Vol. 13, pp. 187-241.

[57]. Oudadesse, H., Bui, X. V. and Yann L.: Chitosan Effects on Bioactive Glass for Application as Biocopmosite Biomaterial. Int J of biolo and biomed engi . 2011; 5: 49-56.

[58]. Oudadesse, H., Mostafa, A. and Bui X. V.: Physico-chemical assessment of biomimetic nano-hydroxyapatite/polymer matrix for use in bony surgery. Int J of biolo and Biomed Engi. 2011; 5: 103-10.

[59]. Mami, M., Lucas-Girot, A. and Oudadesse, H.: Investigation of the surface reactivity of a sol–gel derived glass in the ternary system SiO_2–CaO–P_2O_5 . App Sur Sci 2008; 54:7386–93.

[60]. Bellucci, D., Cannillo, V. and Sola, A.: Macroporous Bioglass®-derived scaffolds for bone tissue regeneration. Ceram Int 2011; 37: 1575–85.

[61]. Gaalen, S.M.V., Kruyt, M.C. and Meijer, G.J.: Tissue engineering of bone, in: C.v. Blitterswijk, J. Sohier (Eds.), Tissue Engineering, Academic Press, Elsevier, UK, 2008, pp. 555–606.

[62]. Gomes, M.E., Azevedo, H.S., Moreira, A.R., Ellä, V., Kellomäki, M. and Reis, R.L.: Starchpoly(- caprolactone) and starch-poly(lactic acid) fibre-mesh scaffolds for bone tissue engineering applications: structure, mechanical properties and degradation behavior. J Tiss Engi Rege Medici. 2008; 2: 243–52.

[63]. Zhang, F., Chuanglong H. and Lijun Cao.: Fabrication of gelatin–hyaluronic acid hybrid scaffolds with tunable porous structures for soft tissue engineering. Int J Biolo Macromolec, 2011; 48: 474–81.

[64]. Wu, F., Liu, Ch. and O'Neill, B.: Fabrication and properties of porous scaffold of magnesium phosphate/polycaprolactone biocomposite for bone tissue engineering. App Surf Sci, 2012; 258:7589–95.

[65]. Peter, M., Binulal, N.S. and Nair, S.V.: Novel biodegradable chitosan–gelatin/nano-bioactive glass ceramic composite scaffolds for alveolar bone tissue engineering. Chem Engi J, 2010; 158:353–61.

[66]. Unnithan, A. R., Barakat, N. A.M. and Tirupathi Pichiah, P.B., Wound-dressing materials with antibacterial activity from electrospun polyurethane–dextran nanofiber mats containing ciprofloxacin HCl. Carbohyd Poly, 2012;90 : 1786–93.

[67]. Wang, Q., Zedong, Du Y. and Kennedy, J.: Controlled release of ciprofloxacin hydrochloride from chitosan/polyethylene glycol blend films. Carbohyd. Polym.2007; 69:336–43.

[68]. Sahoo, S., Charkaborti, Ch. K. and Behera, P. K.: Qualitativ analysis of a ciprofloxacin / HPMC mucoadhesive suspension. Int J Pharma and Bio Sci , 2012; 3: 558-76.

[69]. Rodrı´guez-Tenreiro, C., Alvarez-Lorenzo, C., Concheiro, A. and Torres-Labandeira, J.J.: Characterization of cyclodextrin-carbopol interactions by DSC and FTIR. J Therm Anal Calorim. 2004; 77:403–11.

[70]. Nayak, A. K., Laha, B. and Sen, K. K.: Development of hydroxyapatite-ciprofloxacin bone-implants using Quality by design. Acta Pharm. 2011; 61: 25–36.

[71]. Sunitha , A. and Kumar, S.: Study on Effect of Solvents & Nonsolvents on Microspheres of Ciprofloxacin: Coacervation Phase Separation. J Adv Sci Res, 2010; 1(2): 24-33.

[72]. Sunitha , A. and Kumar, S.: Study on the effect of polymers on the release rate of drug from ciprofloxacin hydrochloride microspheres .J Pharmaceu Cosmetolo 2010;1(1): 1-8.

[73]. Kesavan, S. and Alamelu Bai, S.: Effect of surfactant on the release of ciprofloxacin from gelatin microspheres. J. ARS Pharmaceu Ars Pharm, 2010;51 n 1: 1-16.

[74]. Thakre, Y. M. and Choudhary, M. D.: Synthesis, characterization and evaluation of derivative of Ciprofloxacin (1-cyclopropyl-6-fluoro-4-oxo-7-[4-(phenyl carbonyl) piperazin-1-yl]-1, 4-dihydroquinoline-3-carboxylic acid) and their complexes. J Chem Pharm Res, 2011; 3(5):390-8.

[75]. Puga, A. M., Rey-Rico, A. and Magariños B.: Hot melt poly-e-caprolactone/poloxamine implantable matrices for sustained delivery of ciprofloxacin. Acta Biomate, 2012; 8:1507–18.

Table

Table (1): porosity percentage and pore diameter measured by mercury Hg porosimeter and liquid displacement techniques.

Sample name	pore diameter range (4V/A)		Porosity %				
	µm	nm	MIP	Liquid displacement			
				Without drug	With drug		
					5%	10%	20%
PVA	139	6.2	88.14	85.47	72	69	66
2PVA:1SG-B	131	6.3	74.95	79.46	77	74	73
1PVA:1SG-B	119	6.3	67.60	70.30	70	69	67
1PVA:2SG-B	110	6.3	46.68	60.50	59	58	55

Figures

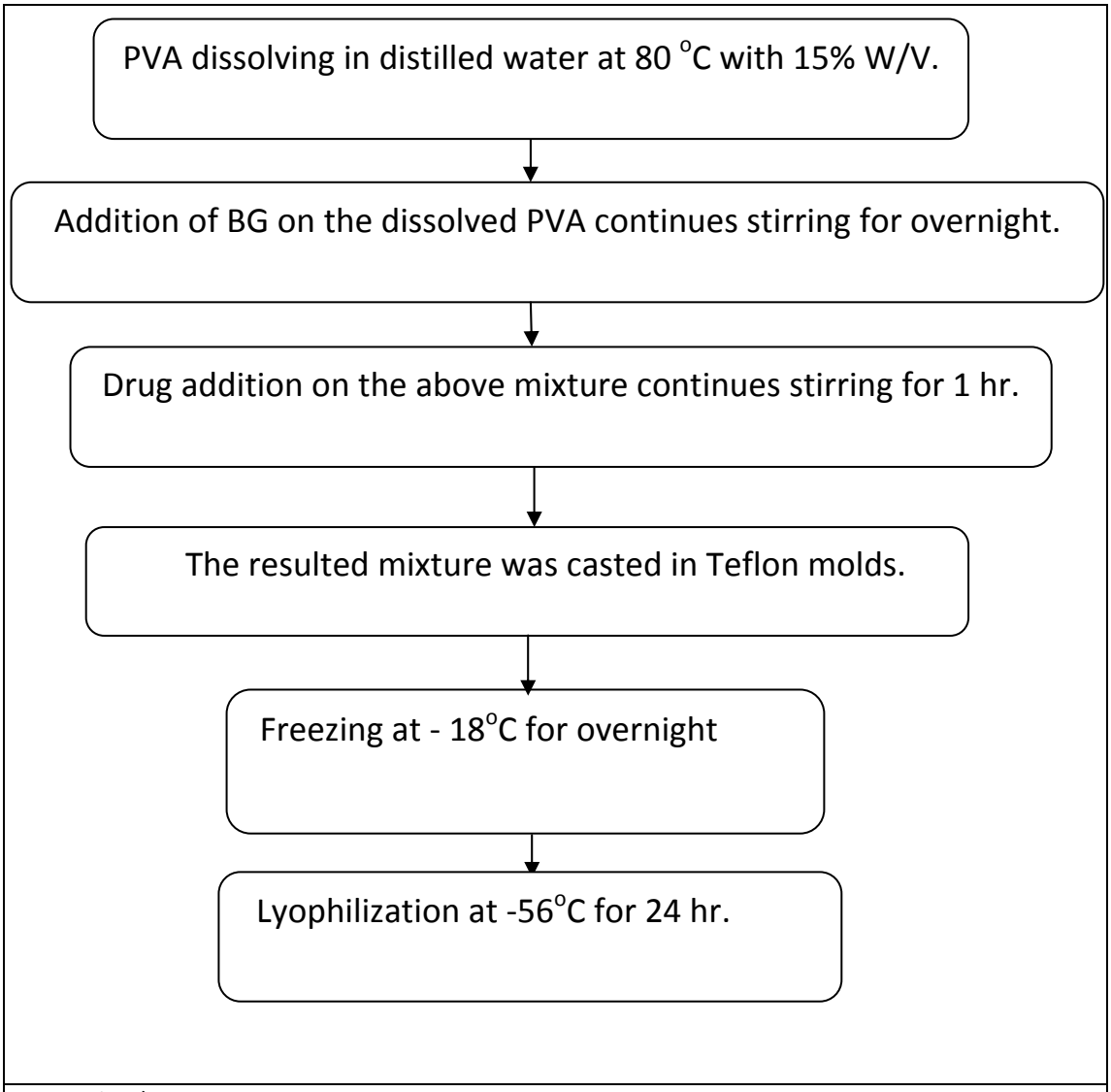

Figure (1.1)

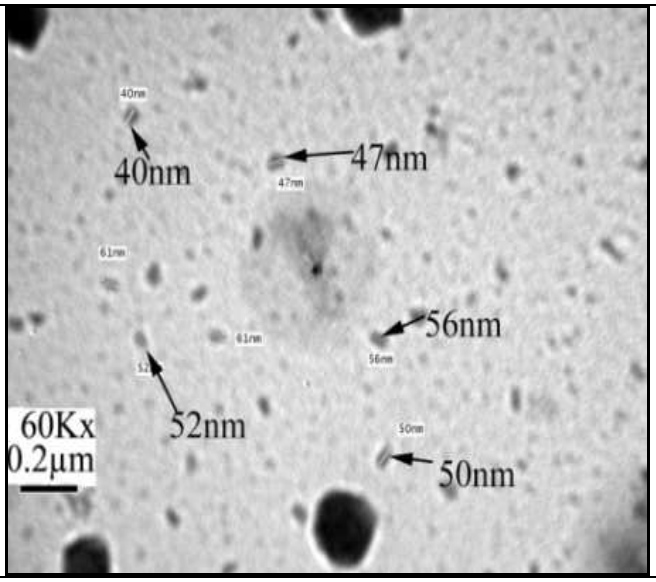

Figure (1.2) TEM image of the prepared glass

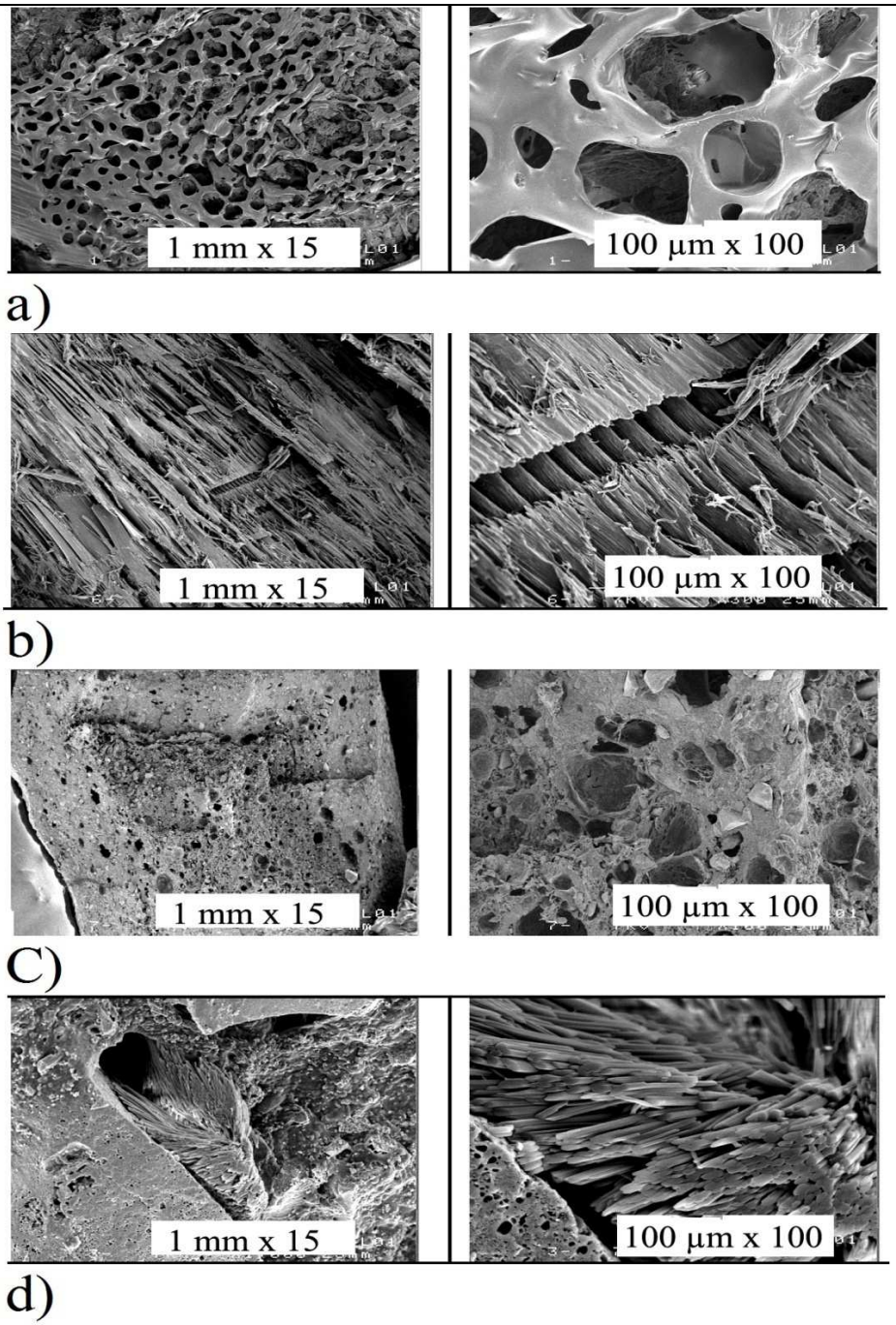

Figure (2) SEM images of a)PVA scaffold , b) PVA scaffold loaded with 20% ciprofloxacin , c) 1PVA:2SG-B and d) 1PVA:2SG-B scaffold loaded with 20% ciprofloxacin

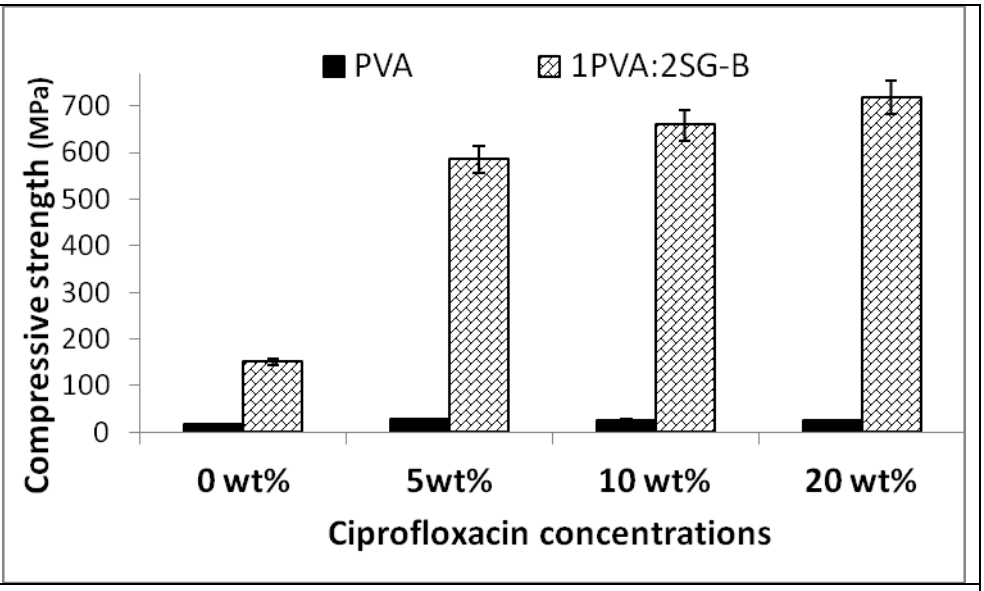

Figure (3) compressive strength of prepared scaffolds

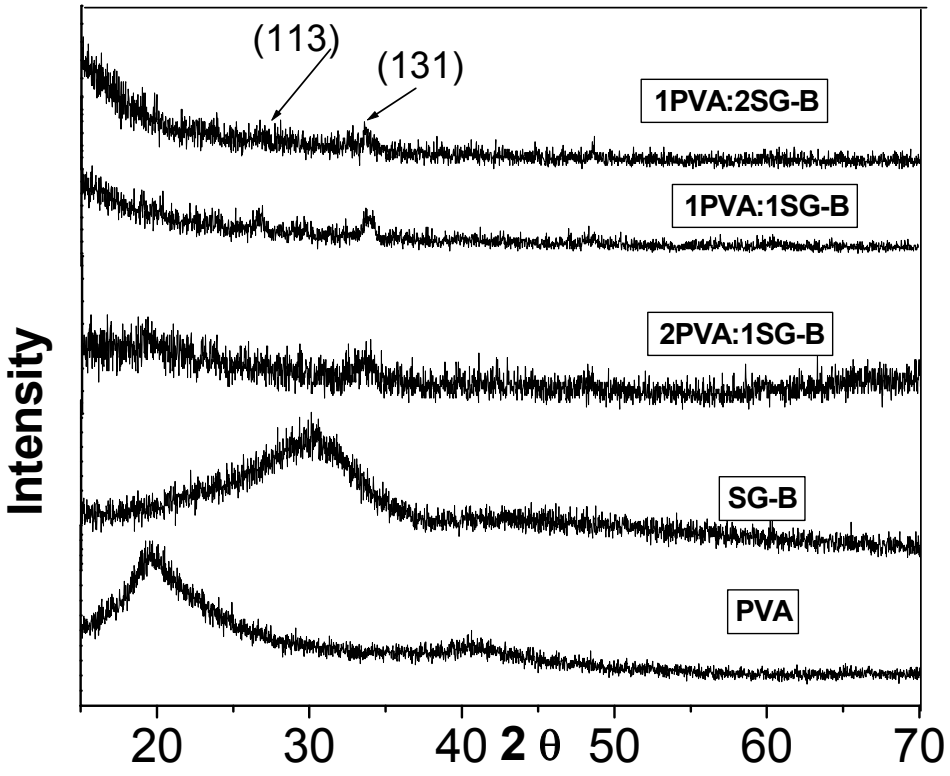

Figure (4) XRD of the prepared scaffolds before immersion in SBF

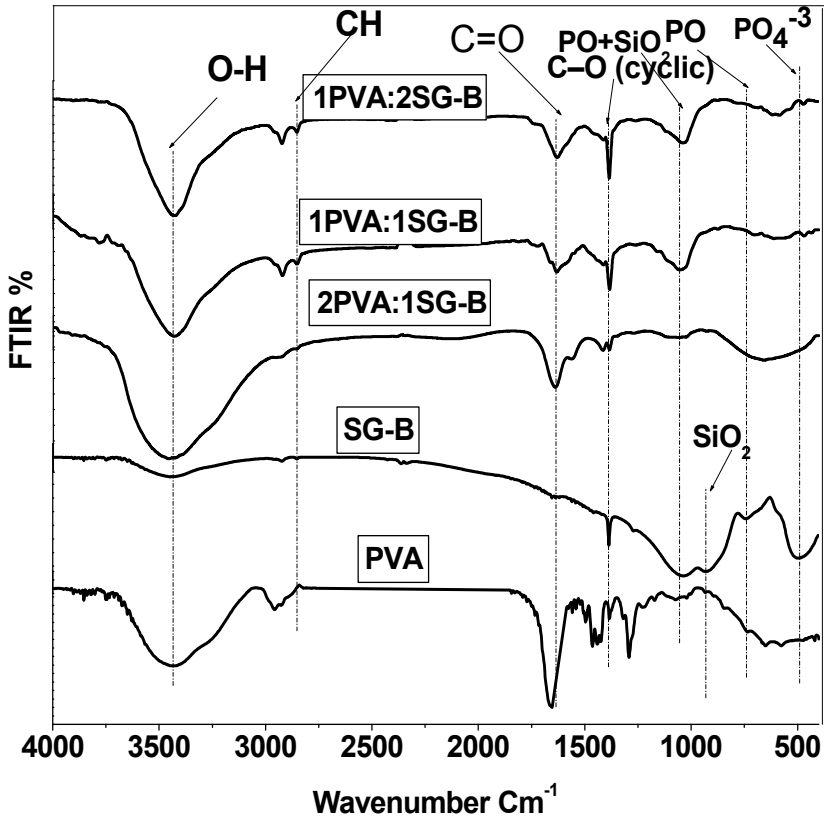

Figure (5) FTIR of the prepared scaffolds before immersion in SBF

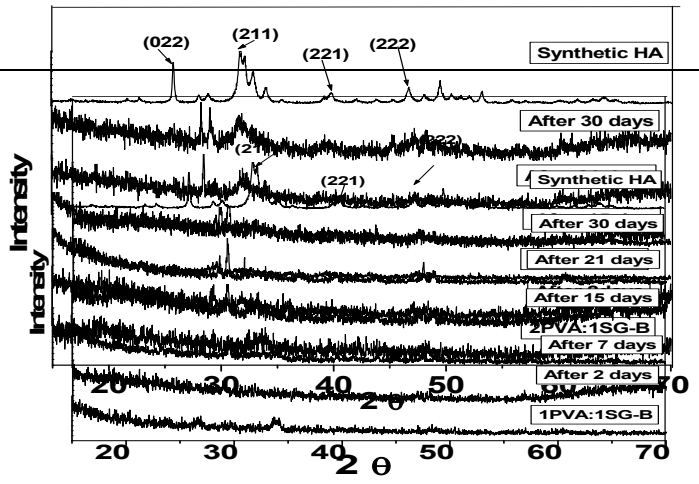

Figure (6.1) XRD of 2PVA:1SG-B after soaking in SBF

Figure (6.2) 1PVA:1SG-B after soaking in SBF

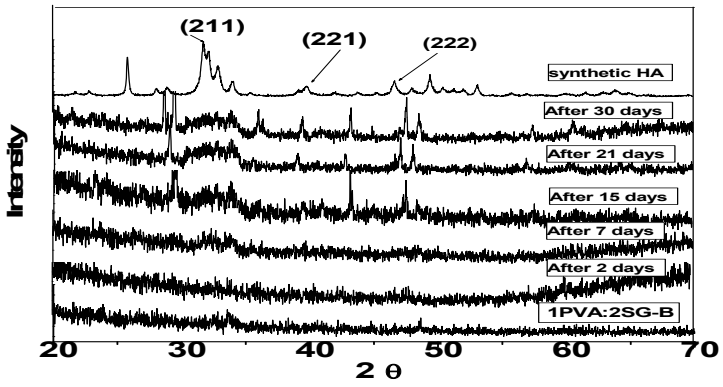

Figure (6.3) 1PVA:2SG-B after soaking in SBF

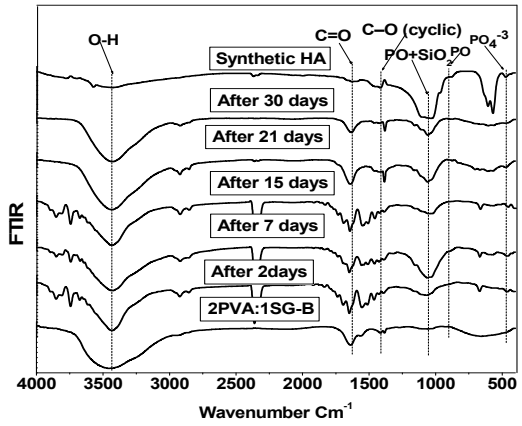

Figure (7.1) 2PVA:1SG-B after soaking in SBF

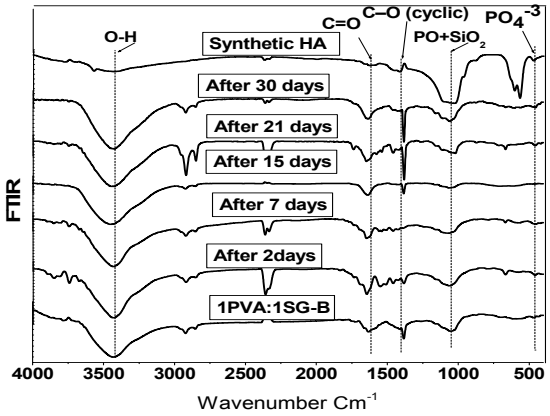

Figure (7.2) 1PVA:1SG-B after soaking in SBF

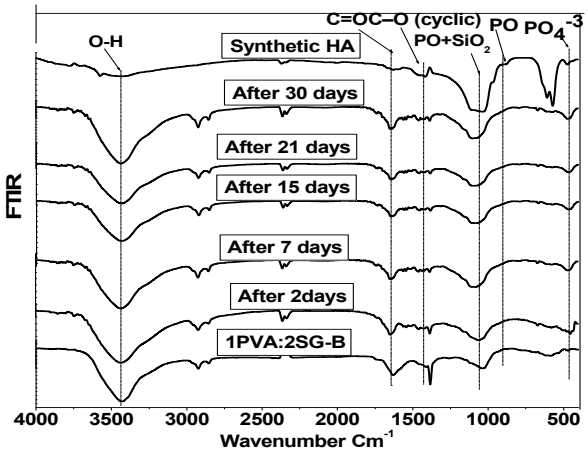

Figure (7.3) 1PVA:2SG-B after soaking in SBF

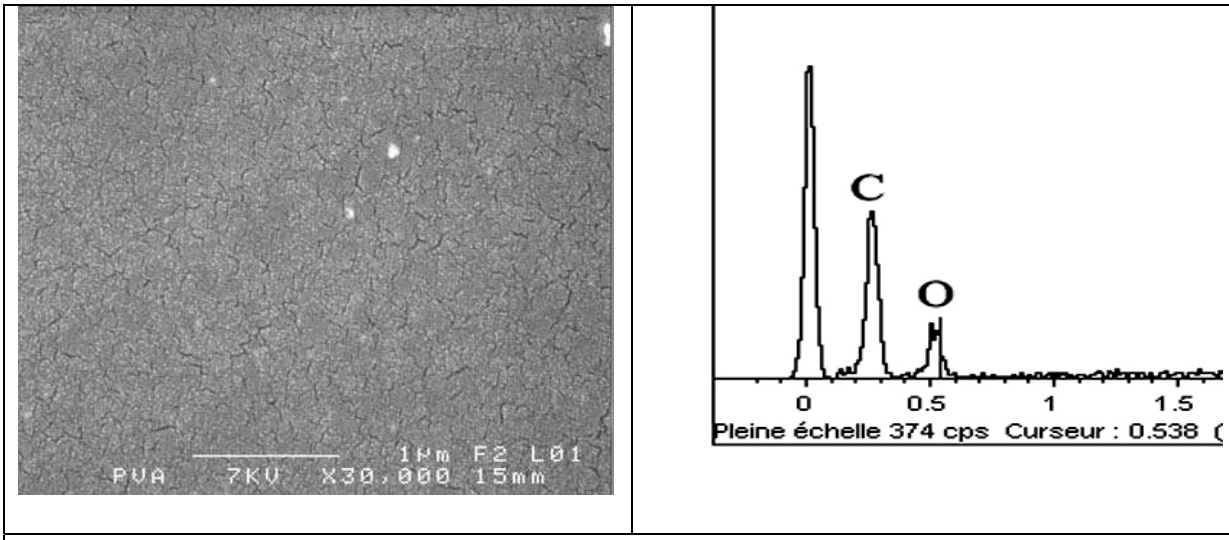

Figure (8.1) SEM with EDS of PVA scaffold after 21 days of immersion in SBF

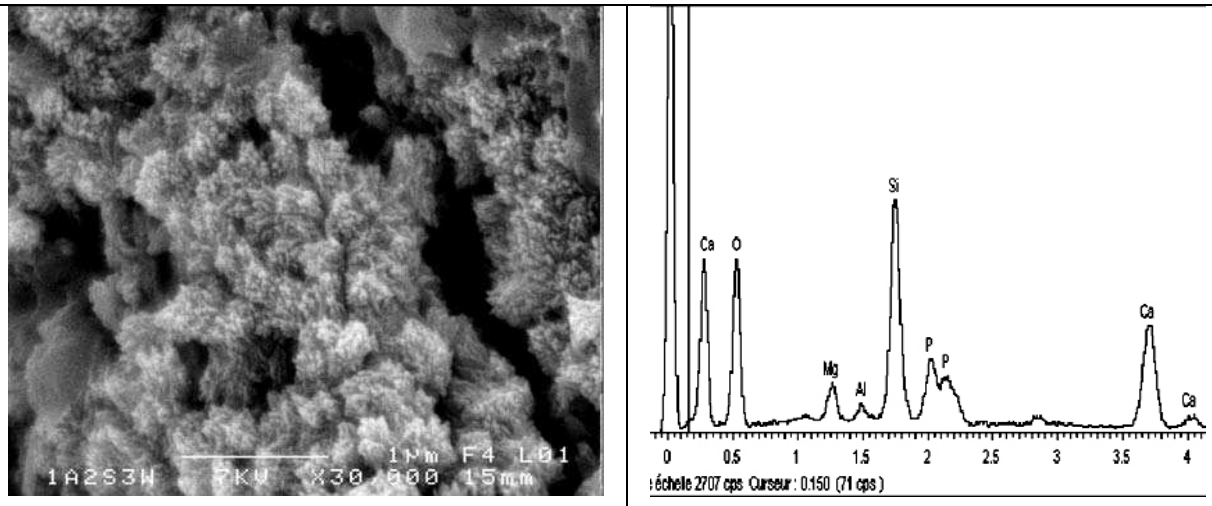

Figure (8.2) SEM with EDS of 1PVA:2SG-B scaffold after 21 days of immersion in SBF

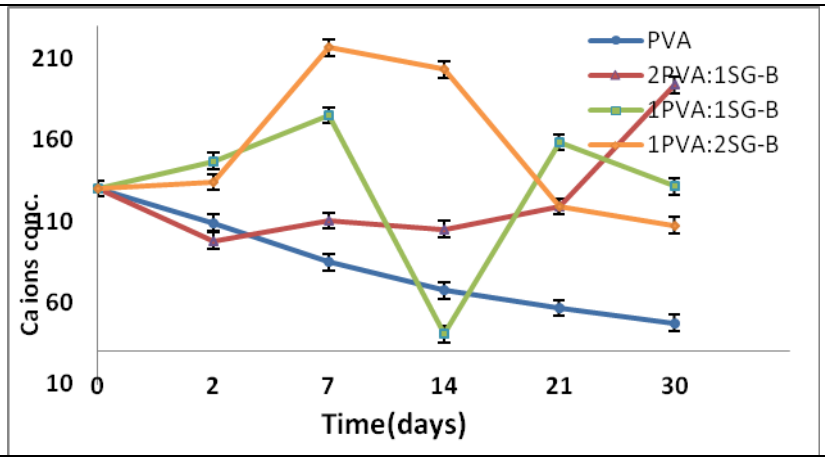

Figure (9.1) Ca ions concentrations after soaking of the prepared Scaffolds in SBF for different times intervals

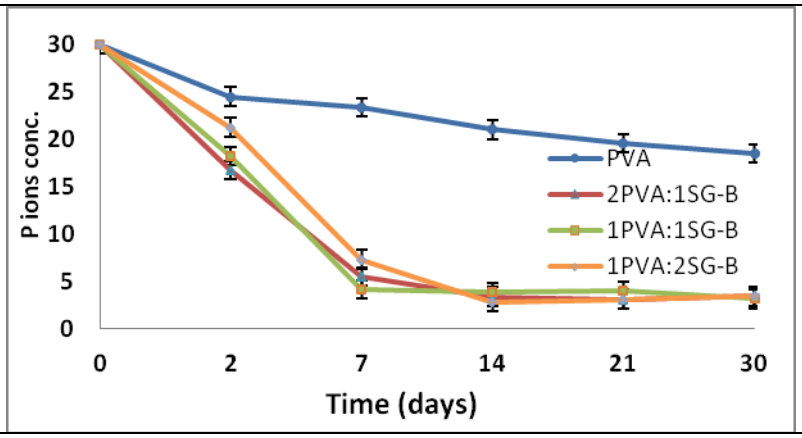

Figure (9.2) P ions concentrations after soaking of the prepared Scaffolds in SBF for different times intervals

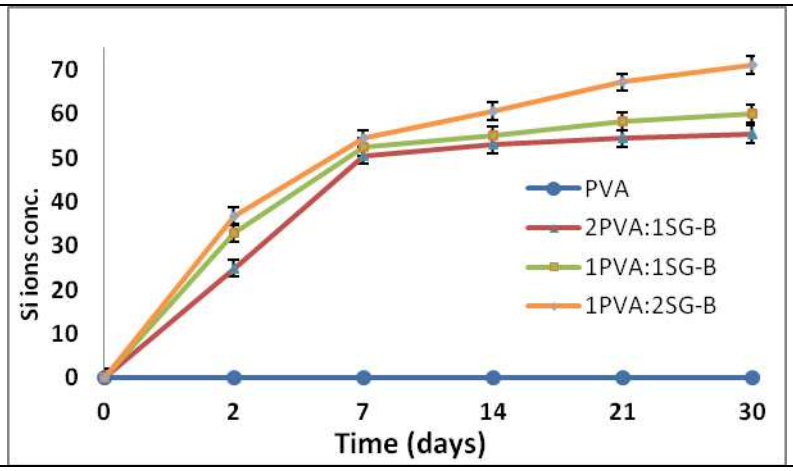

Figure (9.3) Si ions concentrations after soaking of PVA Scaffolds in SBF for different times intervals

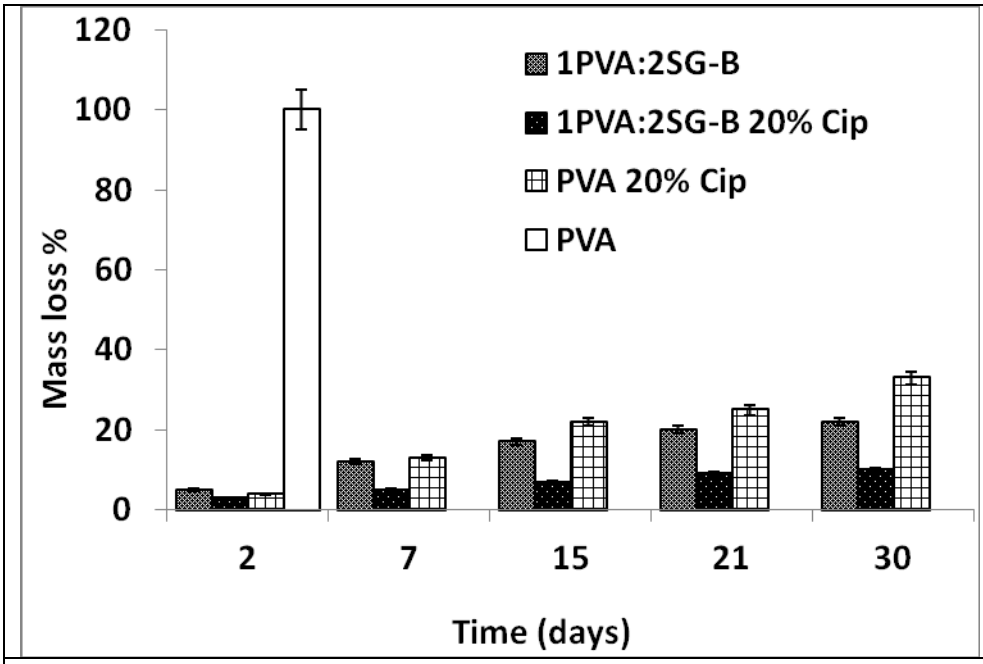

Figure (10) biodegradation rate of the prepared scaffold with and without drug in PBS

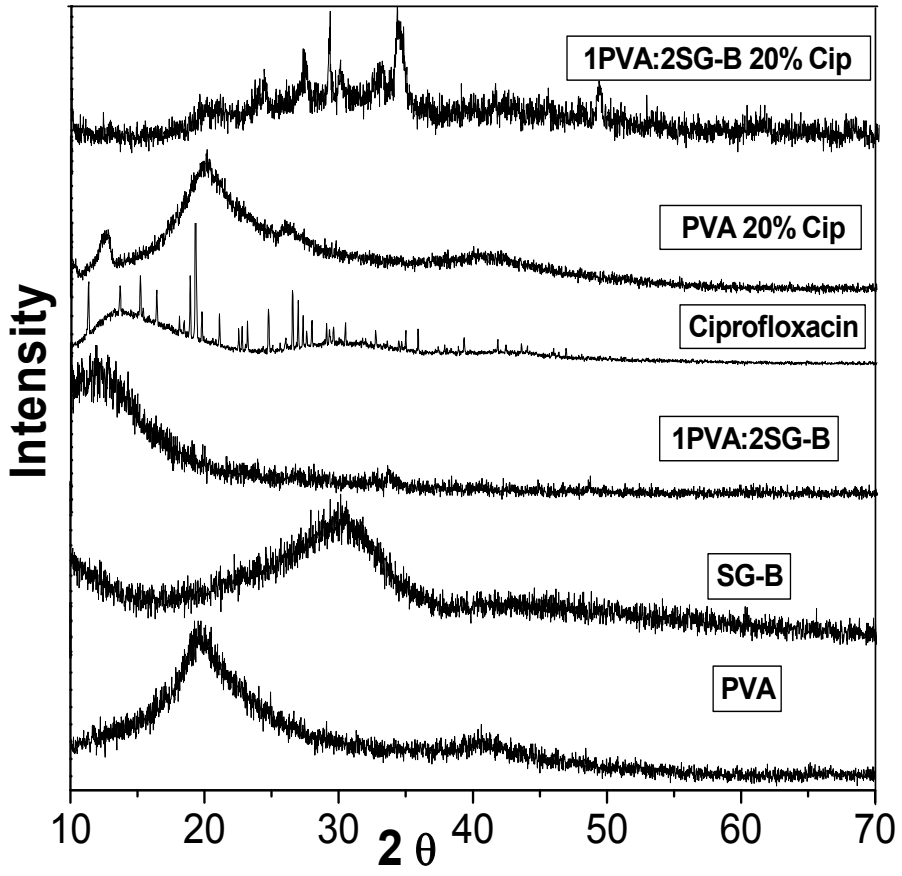

Figure (11.1) XRD of the prepared scaffolds before and after drug incorporation

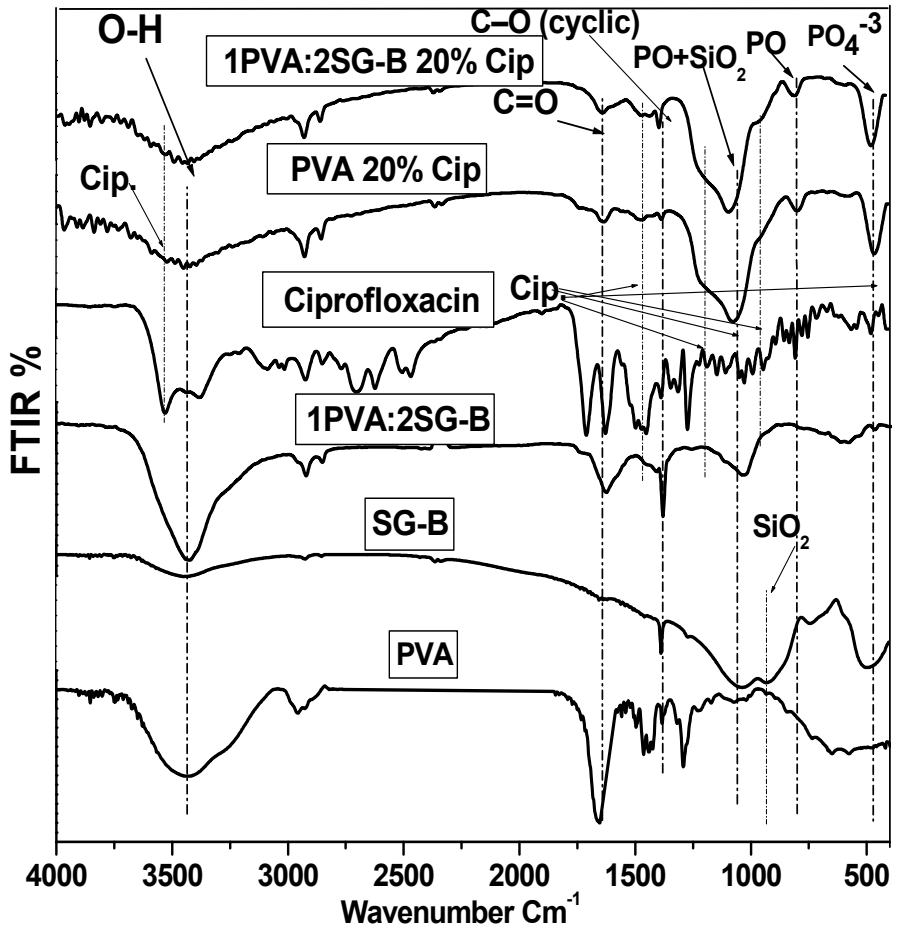

Figure (11.2) FTIR of the prepared scaffolds before and after drug incorporation

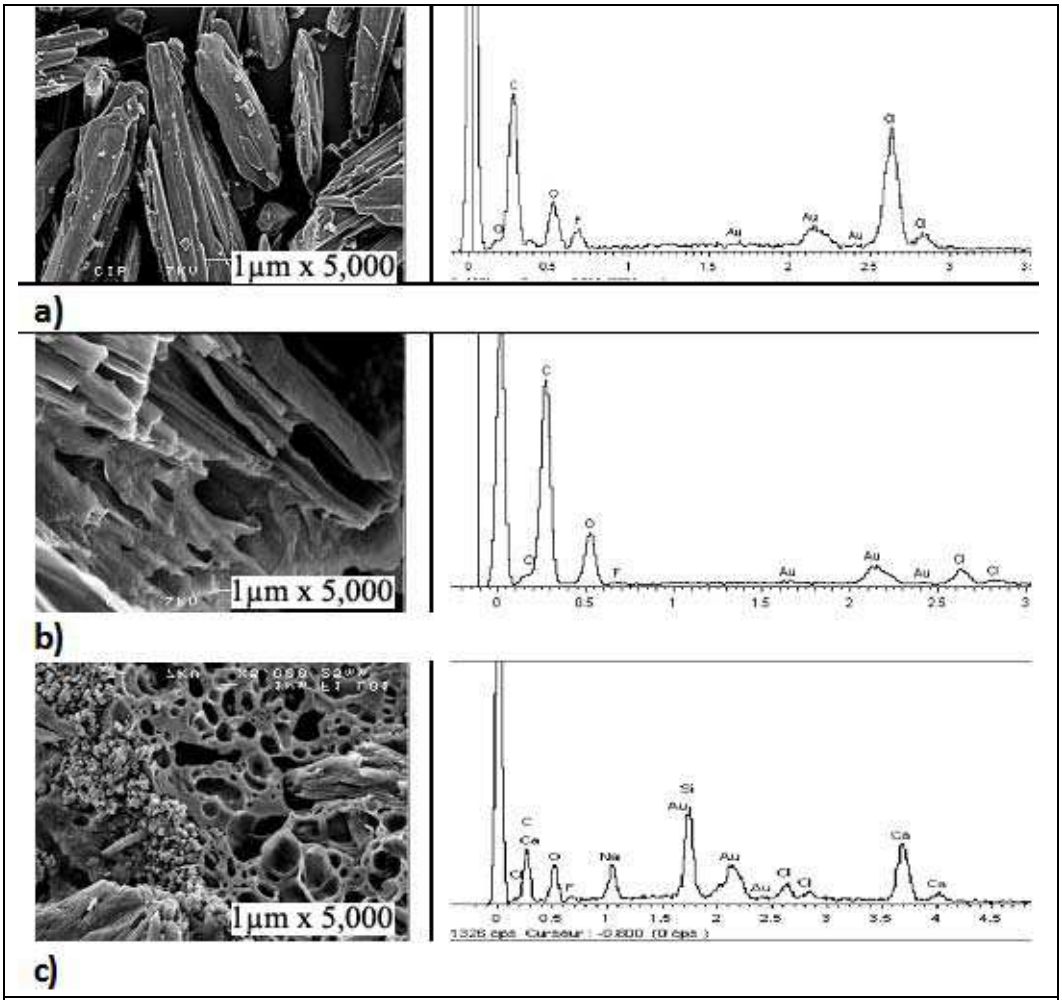

Figure (11.3) SEM with EDS of a) ciprofloxacin , b) PVA scaffold loaded with 20% ciprofloxacin and c) 1PVA:2SG-B scaffold loaded with 20% ciprofloxacin

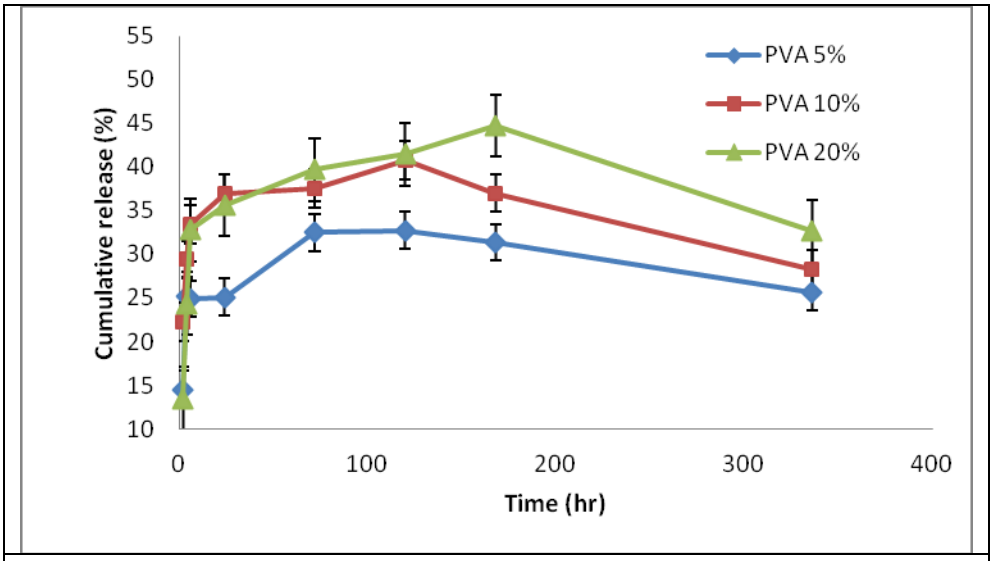

Figure (12.1) cumulative ciprofloxacin release from PVA scaffolds in PBS

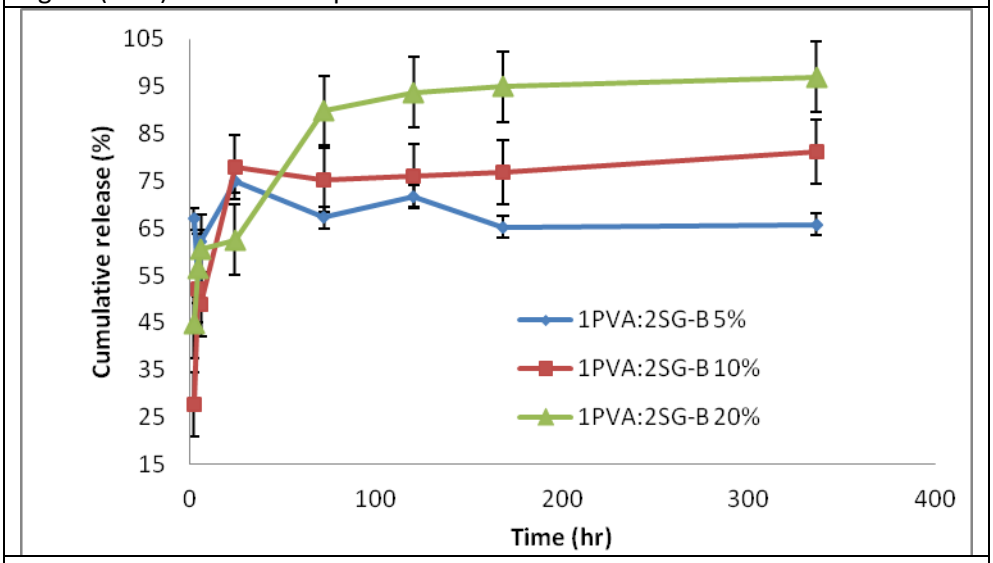

Figure (12.1) cumulative ciprofloxacin release from 1PVA:2SG-B scaffolds in PBS